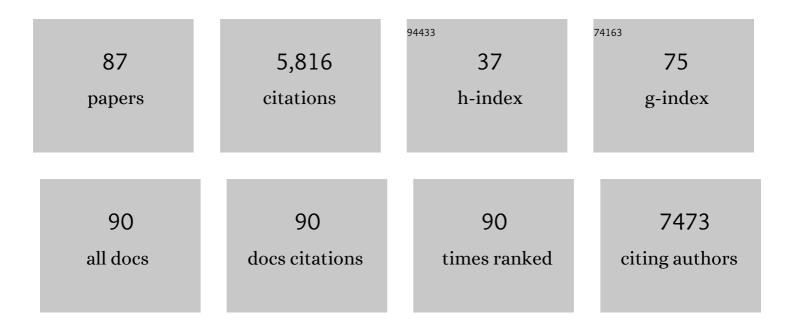
Dehua Xiong

List of Publications by Year in descending order

Source: https://exaly.com/author-pdf/4652813/publications.pdf Version: 2024-02-01



DEHLIA XIONC

#	Article	IF	CITATIONS
1	Bifunctional Nickel Phosphide Nanocatalysts Supported on Carbon Fiber Paper for Highly Efficient and Stable Overall Water Splitting. Advanced Functional Materials, 2016, 26, 4067-4077.	14.9	591
2	Trends in activity for the oxygen evolution reaction on transition metal (M = Fe, Co, Ni) phosphide pre-catalysts. Chemical Science, 2018, 9, 3470-3476.	7.4	443
3	Boosting the hydrogen evolution performance of ruthenium clusters through synergistic coupling with cobalt phosphide. Energy and Environmental Science, 2018, 11, 1819-1827.	30.8	350
4	Hydrothermal Synthesis of Monolithic Co ₃ Se ₄ Nanowire Electrodes for Oxygen Evolution and Overall Water Splitting with High Efficiency and Extraordinary Catalytic Stability. Advanced Energy Materials, 2017, 7, 1602579.	19.5	267
5	Synthesis of the 0D/3D CuO/ZnO Heterojunction with Enhanced Photocatalytic Activity. Journal of Physical Chemistry C, 2018, 122, 9531-9539.	3.1	246
6	The oxygen evolution reaction enabled by transition metal phosphide and chalcogenide pre-catalysts with dynamic changes. Chemical Communications, 2019, 55, 8744-8763.	4.1	246
7	Hierarchical ZnO Decorated with CeO ₂ Nanoparticles as the Direct Z-Scheme Heterojunction for Enhanced Photocatalytic Activity. ACS Applied Materials & Interfaces, 2018, 10, 39679-39687.	8.0	226
8	Fast fabrication of self-supported porous nickel phosphide foam for efficient, durable oxygen evolution and overall water splitting. Journal of Materials Chemistry A, 2016, 4, 5639-5646.	10.3	224
9	From water reduction to oxidation: Janus Co-Ni-P nanowires as high-efficiency and ultrastable electrocatalysts for over 3000Âh water splitting. Journal of Power Sources, 2016, 330, 156-166.	7.8	190
10	Facile synthesis of iron phosphide nanorods for efficient and durable electrochemical oxygen evolution. Chemical Communications, 2016, 52, 8711-8714.	4.1	168
11	Hydrothermal synthesis of ultrasmall CuCrO2 nanocrystal alternatives to NiO nanoparticles in efficient p-type dye-sensitized solar cells. Journal of Materials Chemistry, 2012, 22, 24760.	6.7	162
12	Vapor–solid synthesis of monolithic single-crystalline CoP nanowire electrodes for efficient and robust water electrolysis. Chemical Science, 2017, 8, 2952-2958.	7.4	162
13	SrCl ₂ Derived Perovskite Facilitating a High Efficiency of 16% in Holeâ€Conductorâ€Free Fully Printable Mesoscopic Perovskite Solar Cells. Advanced Materials, 2017, 29, 1606608.	21.0	135
14	Vertically Aligned Porous Nickel(II) Hydroxide Nanosheets Supported on Carbon Paper with Longâ€Term Oxygen Evolution Performance. Chemistry - an Asian Journal, 2017, 12, 543-551.	3.3	118
15	Self-supported Co-Ni-P ternary nanowire electrodes for highly efficient and stable electrocatalytic hydrogen evolution in acidic solution. Catalysis Today, 2017, 287, 122-129.	4.4	105
16	Hollow cobalt phosphide octahedral pre-catalysts with exceptionally high intrinsic catalytic activity for electro-oxidation of water and methanol. Journal of Materials Chemistry A, 2018, 6, 20646-20652.	10.3	95
17	Remarkable photocurrent of p-type dye-sensitized solar cell achieved by size controlled CuGaO ₂ nanoplates. Journal of Materials Chemistry A, 2014, 2, 2968-2976.	10.3	93
18	Atomic-layer-deposited ultrafine MoS ₂ nanocrystals on cobalt foam for efficient and stable electrochemical oxygen evolution. Nanoscale, 2017, 9, 2711-2717.	5.6	88

#	Article	IF	CITATIONS
19	Porous W-doped VO2 films with simultaneously enhanced visible transparency and thermochromic properties. Journal of Sol-Gel Science and Technology, 2016, 77, 85-93.	2.4	85
20	Efficient and durable electrochemical hydrogen evolution using cocoon-like MoS2 with preferentially exposed edges. International Journal of Hydrogen Energy, 2016, 41, 9344-9354.	7.1	74
21	Improved Photovoltages for p-Type Dye-Sensitized Solar Cells Using CuCrO ₂ Nanoparticles. Journal of Physical Chemistry C, 2014, 118, 16375-16379.	3.1	72
22	Synthesis and Characterization of CuAlO ₂ and AgAlO ₂ Delafossite Oxides through Low-Temperature Hydrothermal Methods. Inorganic Chemistry, 2014, 53, 4106-4116.	4.0	70
23	Enhanced Performance of pâ€Type Dyeâ€Sensitized Solar Cells Based on Ultrasmall Mgâ€Doped CuCrO ₂ Nanocrystals. ChemSusChem, 2013, 6, 1432-1437.	6.8	68
24	Template-Free Synthesis of Hollow Iron Phosphide–Phosphate Composite Nanotubes for Use as Active and Stable Oxygen Evolution Electrocatalysts. ACS Applied Nano Materials, 2018, 1, 617-624.	5.0	66
25	Oneâ€Step Fabrication of Monolithic Electrodes Comprising Co ₉ S ₈ Particles Supported on Cobalt Foam for Efficient and Durable Oxygen Evolution Reaction. Chemistry - A European Journal, 2017, 23, 8749-8755.	3.3	64
26	A low temperature hydrothermal synthesis of delafossite CuCoO ₂ as an efficient electrocatalyst for the oxygen evolution reaction in alkaline solutions. Inorganic Chemistry Frontiers, 2018, 5, 183-188.	6.0	58
27	Low-cost porous Cu2ZnSnSe4 film remarkably superior to noble Pt as counter electrode in quantum dot-sensitized solar cell system. Journal of Power Sources, 2013, 226, 359-362.	7.8	57
28	Hydrothermal synthesis of delafossite CuFeO ₂ crystals at 100 °C. RSC Advances, 2015, 5, 49280-49286.	3.6	56
29	Spray deposition of water-soluble multiwall carbon nanotube and Cu2ZnSnSe4 nanoparticle composites as highly efficient counter electrodes in a quantum dot-sensitized solar cell system. Nanoscale, 2013, 5, 6992.	5.6	54
30	Efficient p-type dye-sensitized solar cells based on disulfide/thiolate electrolytes. Nanoscale, 2013, 5, 7963.	5.6	50
31	Crystal structural, optical properties and mott-schottky plots of p-type Ca doped CuFeO 2 nanoplates. Materials Research Bulletin, 2016, 83, 141-147.	5.2	50
32	Modulated Charge Injection in p-Type Dye-Sensitized Solar Cells Using Fluorene-Based Light Absorbers. ACS Applied Materials & Interfaces, 2014, 6, 3448-3454.	8.0	48
33	Polyvinylpyrrolidone-Assisted Hydrothermal Synthesis of CuCoO ₂ Nanoplates with Enhanced Oxygen Evolution Reaction Performance. ACS Sustainable Chemistry and Engineering, 2019, 7, 1493-1501.	6.7	48
34	Bi-metallic cobalt-nickel phosphide nanowires for electrocatalysis of the oxygen and hydrogen evolution reactions. Catalysis Today, 2020, 358, 196-202.	4.4	46
35	High-efficient separation of photoinduced carriers on double Z-scheme heterojunction for superior photocatalytic CO2 reduction. Journal of Colloid and Interface Science, 2020, 564, 303-312.	9.4	46
36	Selective laser sintering of TiO ₂ nanoparticle film on plastic conductive substrate for highly efficient flexible dye-sensitized solar cell application. Journal of Materials Chemistry A, 2014, 2, 4566-4573.	10.3	40

#	Article	IF	CITATIONS
37	Recent progress on tandem structured dye-sensitized solar cells. Frontiers of Optoelectronics, 2012, 5, 371-389.	3.7	39
38	TiO ₂ Nanorods: A Facile Size- and Shape-Tunable Synthesis and Effective Improvement of Charge Collection Kinetics for Dye-Sensitized Solar Cells. ACS Applied Materials & Interfaces, 2014, 6, 9698-9704.	8.0	37
39	Preparation of p-type AgCrO2 nanocrystals through low-temperature hydrothermal method and the potential application in p-type dye-sensitized solar cell. Journal of Alloys and Compounds, 2015, 642, 104-110.	5.5	37
40	One-step fabrication of a self-supported Co@CoTe ₂ electrocatalyst for efficient and durable oxygen evolution reactions. Inorganic Chemistry Frontiers, 2020, 7, 2523-2532.	6.0	37
41	Preparation and characterization of CuCrO2/TiO2 heterostructure photocatalyst with enhanced photocatalytic activity. Applied Surface Science, 2015, 347, 747-754.	6.1	34
42	Low temperature hydrothermal synthesis mechanism and thermal stability of p-type CuMnO ₂ nanocrystals. New Journal of Chemistry, 2016, 40, 6498-6504.	2.8	34
43	Use of delafossite oxides CuCr1-xGaxO2 nanocrystals in p-type dye-sensitized solar cell. Journal of Alloys and Compounds, 2016, 662, 374-380.	5.5	32
44	Highly-ordered silicon nanowire arrays for photoelectrochemical hydrogen evolution: an investigation on the effect of wire diameter, length and inter-wire spacing. Sustainable Energy and Fuels, 2018, 2, 978-982.	4.9	31
45	Cluster Beam Deposition of Ultrafine Cobalt and Ruthenium Clusters for Efficient and Stable Oxygen Evolution Reaction. ACS Applied Energy Materials, 2018, 1, 3013-3018.	5.1	29
46	Passivation of hematite nanorod photoanodes with a phosphorus overlayer for enhanced photoelectrochemical water oxidation. Nanotechnology, 2016, 27, 375401.	2.6	28
47	Investigation of the structural, optical and electrical properties of Ca ²⁺ doped CuCoO ₂ nanosheets. Dalton Transactions, 2019, 48, 13753-13759.	3.3	28
48	A facile hydrothermal route to synthesize delafossite CuMnO2 nanocrystals. Journal of Materials Science: Materials in Electronics, 2015, 26, 10159-10163.	2.2	26
49	Anodic bonding of glass–ceramics to stainless steel coated with intermediate SiO2 layer. Microelectronic Engineering, 2010, 87, 1741-1746.	2.4	24
50	Near Field Enhanced Photocurrent Generation in P-type Dye-Sensitized Solar Cells. Scientific Reports, 2014, 4, 3961.	3.3	24
51	Surfactant-Modified Hydrothermal Synthesis of Ca-Doped CuCoO ₂ Nanosheets with Abundant Active Sites for Enhanced Electrocatalytic Oxygen Evolution. Inorganic Chemistry, 2020, 59, 9889-9899.	4.0	23
52	Oleic acid assisted formation mechanism of CuInS ₂ nanocrystals with tunable structures. RSC Advances, 2014, 4, 36875-36881.	3.6	22
53	Enhanced luminous efficiency of multilayer gradient refractive index phosphor in P2O5-ZnO-B2O3-BaO glass for white light-emitting diode packages. Journal of Non-Crystalline Solids, 2017, 471, 215-221.	3.1	22
54	High refractive index coating of phosphor-in-glass for enhanced light extraction efficiency of white LEDs. Journal of Materials Science, 2018, 53, 1335-1345.	3.7	22

#	Article	IF	CITATIONS
55	Metal–organic framework derived bimetal oxide CuCoO ₂ as efficient electrocatalyst for the oxygen evolution reaction. Dalton Transactions, 2022, 51, 5997-6006.	3.3	22
56	Self-supported cobalt–nickel bimetallic telluride as an advanced catalyst for the oxygen evolution reaction. Inorganic Chemistry Frontiers, 2021, 8, 4247-4256.	6.0	19
57	Fabrication and band engineering of Cu-doped CdSe0.6Te0.4-alloyed quantum dots for solar cells. Solar Energy Materials and Solar Cells, 2016, 157, 161-170.	6.2	18
58	Tunable chromaticity and enhanced luminous efficacy of white LEDs with phosphor-in-glass coating via multilayer screen-printing. Ceramics International, 2017, 43, 13569-13575.	4.8	18
59	Solvothermal synthesis of CuCoO ₂ nanoplates using zeolitic imidazolate framework-67 (ZIF-67) as a co-derived precursor. New Journal of Chemistry, 2019, 43, 15233-15239.	2.8	18
60	Hydrothermal synthesis of delafossite CuScO ₂ hexagonal plates as an electrocatalyst for the alkaline oxygen evolution reaction. Dalton Transactions, 2020, 49, 3519-3524.	3.3	18
61	Gradient refractive index structure of phosphorâ€nâ€glass coating for packaging of white <scp>LED</scp> s. Journal of the American Ceramic Society, 2019, 102, 1677-1685.	3.8	17
62	CoTe ₂ –NiTe ₂ heterojunction directly grown on CoNi alloy foam for efficient oxygen evolution reaction. Inorganic Chemistry Frontiers, 2022, 9, 332-342.	6.0	14
63	Composition and crystallization kinetics of R2O–Al2O3–SiO2 glass–ceramics. Journal of Alloys and Compounds, 2010, 498, 162-167.	5.5	13
64	Discovery of Real‧pace Topological Ferroelectricity in Metallic Transition Metal Phosphides. Advanced Materials, 2020, 32, e2003479.	21.0	13
65	Bifunctional Catalysts: Bifunctional Nickel Phosphide Nanocatalysts Supported on Carbon Fiber Paper for Highly Efficient and Stable Overall Water Splitting (Adv. Funct. Mater. 23/2016). Advanced Functional Materials, 2016, 26, 4066-4066.	14.9	12
66	Mapping the glass forming region and making their phosphorâ€inâ€glass for application in W‣EDs packaging. Journal of the American Ceramic Society, 2020, 103, 5056-5066.	3.8	11
67	Crystallization behaviors of R2O–Al2O3–SiO2 glass–ceramics for use as anodic bonding materials. Journal of Alloys and Compounds, 2010, 507, 531-534.	5.5	10
68	P-type transparent conducting characteristics of delafossite Ca doped CuScO ₂ prepared by hydrothermal synthesis. Dalton Transactions, 2021, 50, 5262-5268.	3.3	10
69	Heat-up and gram-scale synthesis of Cu-poor CZTS nanocrystals with controllable compositions and shapes. CrystEngComm, 2017, 19, 2013-2020.	2.6	9
70	Self-Epitaxial Hetero-Nanolayers and Surface Atom Reconstruction in Electrocatalytic Nickel Phosphides. ACS Applied Materials & Interfaces, 2020, 12, 21616-21622.	8.0	9
71	Effect of nickel doping on the structure, morphology and oxygen evolution reaction performance of Cu-BTC derived CuCoO ₂ . Dalton Transactions, 2022, 51, 8757-8765.	3.3	9
72	Surface and interface characterization of oxygen plasma activated anodic bonding of glass–ceramics to stainless steel. Microelectronics Reliability, 2012, 52, 1367-1372.	1.7	8

#	Article	IF	CITATIONS
73	Nanocrystals of CuCoO ₂ derived from MOFs and their catalytic performance for the oxygen evolution reaction. Dalton Transactions, 2022, 51, 11536-11546.	3.3	8
74	Electrical properties of R2O–Al2O3–SiO2 glass–ceramics for anodic bonding. Journal of Materials Science: Materials in Electronics, 2010, 21, 882-888.	2.2	7
75	Low-temperature solution synthesis of a ZnO nanorod array with a mesoporous surface mediated by cadmium ions. CrystEngComm, 2016, 18, 8277-8283.	2.6	7
76	Enhanced high reflectance SiO2-Ag-SiO2 thin film adhesion for Concentrating Solar Power reflector. Surfaces and Interfaces, 2017, 8, 225-229.	3.0	7
77	Impact of Mg doping on the optical and electrical properties of p-type CuMnO2 ultrathin nanosheets. Journal of Materials Science: Materials in Electronics, 2020, 31, 5452-5461.	2.2	7
78	Glass forming region and bonding mechanism of lowâ€melting V ₂ O ₅ –TeO ₂ –Bi ₂ O ₃ glass applied in vacuum glazing sealing. Journal of the American Ceramic Society, 2021, 104, 5050-5066.	3.8	7
79	Improved efficiency and carrier dynamic transportation behavior in perovskite solar cells with CuInS ₂ quantum dots as hole-transport materials. Dalton Transactions, 2021, 50, 8837-8844.	3.3	6
80	Controllable synthesis of CdSe/ZnS core–shell quantum dots by one-step thermal injection and application in light-emitting diodes. Journal of Materials Science: Materials in Electronics, 2021, 32, 22024-22034.	2.2	6
81	Hydrothermal synthesized delafossite CuGaO2 as an electrocatalyst for water oxidation. Frontiers of Optoelectronics, 2022, 15, 1.	3.7	6
82	One-step synthesis of novel Ag/AgCl-glass with remarkably stable photocatalytic activity. Journal of Non-Crystalline Solids, 2019, 506, 21-27.	3.1	5
83	Exceptional lithium storage performance achieved by iron-based nanostructures upon extended high-rate cycling. Journal of Alloys and Compounds, 2021, 888, 161626.	5.5	4
84	Enhanced vacuum glazing bonding strength by anodic bondingâ€assisted sealing method. International Journal of Applied Class Science, 2020, 11, 147-154.	2.0	3
85	Al–Si Thin Films Assisted Anodic Bonding of R2O–Al2O3–SiO2 Glass–Ceramics to Stainless Steel. Journal of Adhesion Science and Technology, 2011, 25, 1925-1935.	2.6	2
86	Preparation and Luminescent Properties of Tb3+-doped SrO–Al2O3–SiO2 Glass–Ceramics for white Light-Emitting Diode. Glass Physics and Chemistry, 2018, 44, 300-306.	0.7	1
87	Dye-sensitized Solar Cells Based on P-type Delafossite Structure Nanocrystals of CuCrO2 and CuGaO2. , 2013, , .		0